Original Article

WM&R

Waste Management & Research
1–9

DOI: 10.1177/0734242X17721343
journals.sagepub.com/home/wmr
SAGE

New fired bricks based on municipal solid waste incinerator bottom ash

R Taurino[1,2], E Karamanova[3], L Barbieri[1], S Atanasova-Vladimirova[3], F Andreola[1] and A Karamanov[3]

Abstract

The main objective of this work was to study the sintering process and technological properties of new fired bricks based on high amount of post-treated municipal solid waste incinerator bottom ash and refractory clay. In addition, the effect of the minor addition of flux (Na_2CO_3) or reinforce (corundum) was also highlighted.

Several methods were used to study the effect of compositions variations on the sintering process, structure and the mechanical characteristics of the test briquettes. Differential thermal analysis (TG/DTA) and dilatometry techniques were applied to study the thermal behaviour while scanning electron microscopy coupled with energy-dispersive X-ray spectroscopy and high-temperature X-ray diffraction were used to elucidate the structure and the phase composition. The mechanical characteristics were estimated by micro-indentation, strength and various physical tests (porosity, linear shrinkage and water absorption, etc).

The results highlight the possibility to use very high amount of municipal solid waste incinerator bottom ashes in the production of new fired bricks with good performances at all levels.

It is also shown that the addition of additives managed the final properties, affecting the crystal phase formation, porosity and greatly the strength of the samples.

Keywords

Bricks, bottom ash, sintering process, physical-mechanical properties, microstructure analysis

Received 5th April 2017, accepted 22nd June 2017 by Associate Editor Dimitris Dermatas.

Introduction

Since the construction industry still uses a large amount of clay bricks in buildings, several studies have been made to incorporate coal fly ash, bottom ash (BA) and other residues in the production of fired bricks (Sena da Fonseca B et al., 2015; Aineto et al., 2006; Little et al., 2008; Lingling et al., 2005; Sokolar and Vodova, 2011; Demir, 2006) to contribute to conserve traditional raw materials and to avoid waste disposal (Naganathan et al., 2011). In this context, because of limited landfill sites on the one hand and the presence of silicon, calcium, aluminium and iron in BA on the other hand, municipal solid waste incinerator (MSWI) BAs are now used in the ceramic and building sector as opposed to landfill disposal (Naganathan et al., 2011). In 2004, 2.4 million tonnes of municipal solid waste (MSW) were disposed of by incinerators only in Italy (Aloisi et al., 2006; ISPRA, 2008). This situation demands that the construction industry stakeholders investigate new alternative materials and to develop novel methodologies for effective use of wastes produced from MSW incineration.

Therefore, the development of innovative fired bricks based on a huge amount of MSWI BA can be a substantial step towards the decrease of pollution and environmental impact.

Since MSWI ash contains CaO, SiO_2, Fe_2O_3 and Al_2O_3, a number of studies have investigated their feasibility in the production of mortar and concrete (Pan et al., 2008; Huang and Chu, 2003). Mandal and Sinha (2017a) studied the effect of BA finesse on the properties of red mud geopolymer. Bricks with higher strength and density values with increasing temperature, fineness of BA and iron slime content have been obtained Mandal and Sinha (2017b). Moreover, in a previous work the authors showed the feasibility to use a high amount of post-treated BA (60 wt%) as an alternative raw material in clay-based ceramics compositions.

[1]Department of Engineering "Enzo Ferrari", University of Modena and Reggio Emilia, Modena, Italy
[2]Dipartimento di Ingegneria e Architettura, Università di Parma, Parma, Italy
[3]Institute of Physical Chemistry, Bulgarian Academy of Sciences, Sofia, Bulgaria

Corresponding author:
R Taurino, Dipartimento di Ingegneria e Architettura, Università di Parma, Parco Area delle Scienze 181/A, 43124 Parma, Italy.
Emails: rosa.taurino@unipr.it

Even though in recent years, the partial substitution of clay in bricks by several types of waste has been investigated focusing on the physical and mechanical properties of bricks, (Lingling et al., 2005; Demir, 2006; Pan et al., 2008; Huang and Chu, 2003; Mandal and Sinha, 2017a; Mandal and Sinha, 2017b; Shabback et al., 2012; Muñoz et al., 2016; Martínez-García et al., 2012; Menezes et al., 2005; He et al., 2012; Monteiro, 2005; Raut et al., 2012; Sena da Fonseca et al., 2011; Pérez-Villarejo et al., 2012; Barbieri et al., 2013), extensive experimental studies related to detailed studies of a densification process, phase transformation and microstructures are very limited. Moreover, no information on the effects of additions of reinforcements (as corundum) or intensive fluxes (as Na_2CO_3) in fired clay bricks based on MSWI has been reported.

Generally, similar additives are used to improve some properties of ceramic batches, such as shaping characteristics, drying behaviour, firing behaviour, etc. (Cultrone et al., 2005). Corundum is a raw material with high physical and mechanical properties, which is used in glazes and ceramic materials to increase their mechanical and physical properties (Asenov et al., 2013). Na_2CO_3 is an additive widely used in the glass industry, since it, as foaming agent, affects the density and porosity and additionally enables bathes to sinter at a lower temperature (Mular et al., 2002).

For this purpose, the article examined the densification process and the related phase transformation of bricks made of clay and secondary raw materials from MSWI BA, as well as the supplementary effect of the addition of small amounts (5 wt%) of corundum (Al_2O_3) and sodium carbonate (Na_2CO_3). First, the study was based on the evaluation of the optimal heat-treatment by optical dilatometer and differential thermal analysis. The elemental and phase composition fraction of fired bricks were determined by energy dispersion spectroscopy (EDS) and X-ray diffraction (XRD). The use of scanning electron microscopy (SEM) allowed the capturing of microstructural features. Furthermore, physical and mechanical at micro- and macroscale properties of these heterogeneous materials were investigated and reported.

In the present research, a pre-treated BA and commercialised as 'end of waste material', according to the European Norm 2008/98/CE, was used in the production of new fired bricks. The mechanical pre-treatment process is composed of three steps: (i) aging in open air, (ii) grinding in a mill (obtaining different grain sizes 0–2; 2–8 mm) and (iii) separation of iron and aluminium pieces by means of magnetic and eddy current systems. Nowadays, this inert material is exploited in many sectors of construction material, such as cement (in clinker production), concrete, ceramic product (tiles and bricks) and bituminous conglomerate. Then the incorporation of such BA into the bricks would pose no risk at all, as discussed in other works (Shabback et al., 2012; Dermates and Meng, 2003).

Materials and methods

Materials

The raw material used in this study is an artificial silica-based aggregate, derived from a MSWI BA treatment plant in the North of Italy. Other raw materials, used for the production of bricks, were industrial kaolin (K)-ceramic grade (Balco, Italy), sodium carbonate (Na_2CO_3) and corundum (Al_2O_3) purchased from Sigma–Aldrich Chemical Co.

Table 1. Chemical composition (wt%) of the used raw materials.

Oxides	Kaolin	BA	BA-b
SiO_2	52.5	46.8	48.7
TiO_2	0.5	0.7	0.8
Al_2O_3	33.3	9.8	10.2
Fe_2O_3	0.6	4.3	4.5
CaO	0.2	18.6	19.3
MgO	0.4	2.9	3.0
K_2O	0.9	1.0	1.0
Na_2O	0.1	4.5	4.7
B_2O_3	0	0.6	0.6
MnO	0	0.3	0.3
ZnO	0	0.3	0.3
PbO	0	0.3	0.3
SO_3	0	1.0	1.0
P_2O_3	0	1.2	1.3
CuO	0	0.5	0.5
Others	0	0.2	0.2
L.O.I	11.7	7.1	3.2

BA: bottom ash; L.O.I: loss of ignition.

Table 2. Mineralogy of kaolin (K) and BA used in the mixtures.

Materials	Crystalline phases (ICDD)
Kaolin	Quartz, SiO_2 [01–085–0457] Kaolinite, $Al_2 (Si_2O_5) (OH)_4$ [01–078–1996] Illite, $(K, H_3O) Al_2Si_3AlO_{10} (OH)_2$ [026–0911]
BA	Quartz, SiO_2 [01–085–0794] Calcite, $CaCO_3$ [024–0027] Akermanite-Gehlenite, $Ca_2(Mg_{0.5}Al_{0.5})(Si_{1.5}Al_{0.5}O_7)$ [01–079–2423] Albite calcian ordered, (Na,Ca) Al $(Si, Al)_3O_8$ [041–1480] Covellite, CuS [03–065–3928]

The results of the chemical analysis (determined by Inductively Coupled Plasma, ICP, Varian Liberty 200) of the raw materials (in oxides wt%, experimental error ±0.05 wt%) are reported in Table 1, while their mineralogical compositions, are reported in Table 2. The data elucidated that kaolin has a typical composition for this type of clay. At the same time, the chemical and physical composition of ash will depend on the compositions of raw MSW, the operational conditions, the incinerator and air pollution control system design (He et al., 2004). The BA used in this study, received from an industrial plant located in the North of Italy, is composed of silica, alumina, calcium oxide, sodium oxide and iron in different amounts. SiO_2 is the most abundant compound that exists in BA, containing up to 45 wt%. After heating at 600 °C and burnout of the residual organic part in BA (at about 4 wt%), a small increase in inorganic oxides content is measured in BA material.

Table 3 reports the leaching test results performed on the BA, according to UNI EN 12457-2 (2002). The pH, conductivity and leaching values for all metals and anions were lower than values reported in Decree Ministerial 27/9/2010 (eluate limits for residues to landfill).

Particle size distribution of kaolin in Figure 1 was obtained by laser diffraction using a Malvern Mastersizer (Malvern Instruments, UK). This indicates that the as-received clay has an average particle size (d_{50}) of approximately 7 µm.

The range of apparent particle density on an oven-dried basis of AB was 1.9–2.1 g cm^{-3} and of kaolin was 1.8–2.5 g cm^{-3}.

Samples preparation

All the parent ceramic batches, reported in Table 4, were prepared by mixing the raw materials, grounding, milling and sieved below 75 µm. Each batch was prepared by dry-grinding in ball jar for 10 min and humidified with 6 wt% of distilled water, then green samples were uniaxially pressed at 40 MPa. The samples used with a gauge length of 50 mm and cross section of 5 × 4 mm^2 were used for sintering study (thermal analysis) and in the evaluation of technological properties, such as density and water absorption. Testing cylindrical samples, for mechanical tests, with 18 mm diameter and 36 mm length, were manufactured by compressing at 40 MPa.

The mixing ratio of BA and kaolin of 55:45 was selected to obtain a ceramic batch with a higher content of $CaCO_3$ with respect to the kaolin. In fact, as reported by several researchers (Peters and Iberg, 1978; Cultrone et al., 1998), carbonates can lead to a reduction in shrinkage, anisotropic behaviour and to an increase in compressive strength.

The first ceramic (labelled C) was obtained by mixing 55 wt% 'as it is' BA with 45 wt% kaolin. The second composition (labelled C-b) was prepared using 55 wt% BA, preliminary heat-treated for 2 h at 600 °C (BA–b) (in order to eliminate entirely the residual organic phase) and 45 wt% kaolin. Moreover, in the ceramic batches, labelled C–b–Al and C–b–Na, 5 wt% of BA–b was substituted by fine Al_2O_3 and Na_2CO_3, respectively. The chemical compositions of these four ceramics, determined by X-ray fluorescence analysis (XRF) (ARL ADVANT'XP X-ray fluorescence spectrometer, Thermo Fischer Scientific Inc., Waltham, MA, experimental error ±0.1 wt%) are summarised in Table 4. These samples were dried overnight at 110 °C before the thermal analysis.

Table 3. Leaching test results of MSWI BA used in this work.

Metals/ Anions	BA (mg L^{-1})	Italian limit D.M 27/9/2010 not hazardous waste (mg L^{-1})
Cu	0.480	5.0
Zn	0.191	5.0
Ni	0.050	1.0
As	<0.05	0.2
Cd	0.008	0.02
Cr total	<0.001	1.0
Pb	0.530	1.0
Al	90.40	—
Fe	8.653	—
Na	151.00	—
Cl-	200	2500
SO_4^{2-}	375	5000
pH	10.68	5–12
S.C (µS cm^{-1})	1500	—

Samples characterisation

The sintering process was studied with a horizontal contactless optical dilatometer (Expert System Solutions, Misura HSML ODLT 1400) using a heating rate of 20 °C min^{-1} in the temperature range of 20 °C–1300 °C. The temperature precision given by the equipment is ± 1 °C (Paganelli, 1997).

The phase transformations were followed by differential thermal analysis (TG/DTA, Netzsch STA 409) using the same conditions. The temperature precision given by the equipment is ±5 °C.

The fired bricks mineralogical compositions were evaluated by a conventional Bragg-Brentano powder diffractometer (X'Pert PRO, Panalytical) with nickel -filtered copper Kα radiation using bracket holder. The spectra were collected over 2θ intervals ranging from 10° to 40°, with a step size 0.02° and

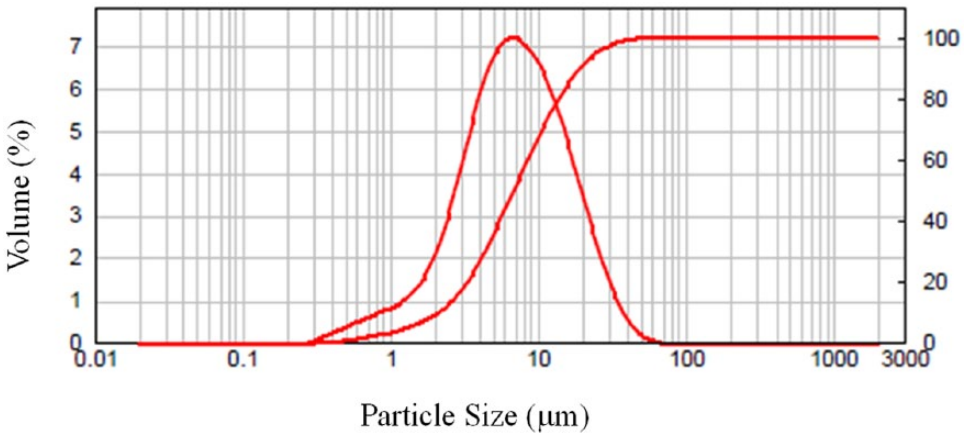

Figure 1. Particle size distribution of kaolin.

Table 4. Chemical composition (wt%) of the studied ceramic batches.

Oxides	C	C-b	C-b-Al	C-b-Na
SiO_2	54.4	54.2	51.5	52.7
TiO_2	0.7	0.7	0.7	0.7
Al_2O_3	22.5	22.2	26.9	22.1
Fe_2O_3	2.9	3.1	2.7	2.8
CaO	11.4	11.6	10.5	10.7
MgO	2.0	2.0	1.8	1.8
K_2O	1.1	1.0	1.0	1.0
Na_2O	2.8	2.8	2.6	5.9
B_2O_3	0.4	0.4	0.3	0.3
MnO	0.2	0.2	0.2	0.2
ZnO	0.2	0.2	0.2	0.2
PbO	0.2	0.2	0.2	0.2
SO_3	0.6	0.6	0.5	0.5
P_2O_3	0.7	0.8	0.7	0.7
CuO	0.3	0.3	0.3	0.3

time step of 25 s. Moreover, to analyse the formation of crystalline phases as a function of the temperature, a high-temperature X-ray diffractometer with a heating chamber (HTK 16) was used. Powders of mixtures (<38 μm) were heated on a platinum bar from room temperature to 900 °C and 1000 °C, where the XRD scanning was performed. The identification of crystalline phases was made under comparison with data on the JCPDS files.

The microstructure and crystal morphology of the fired samples were observed by SEM (JEOL JSM 6390) coupled with EDS equipment (EDS, INCA 350, Oxford). Before metallisation with gold, chemical etching with 2% hydrofluoric acid for 5 s was carried out.

Linear shrinkage (LS%), water absorption (WA%) and measurement of weight loss of ignition (WLOI%) of the fired samples were performed according to ISO 10545-3 (1995).

The apparent density, ρ_a, skeleton, ρ_s and absolute, ρ_{as}, densities of the sintered samples were determined and the results were used to evaluate total P_T, closed P_C and open P_O porosity:

$$P_T = 100 \text{ x } (\rho_{as} - \rho_a) / \rho_{as} \quad (1)$$

$$P_C = 100 \text{ x } (\rho_{as} - \rho_s) / \rho_{as} \quad (2)$$

$$P_O = 100 \text{ x } (\rho_s - \rho_a) / \rho_{as} \quad (3)$$

ρ_a was estimated by an Envelope Density Analyser (GeoPyc 1360, Micrometrics) using a dry-flow medium, while ρ_s and ρ_{as} by gas (Ar) pycnometer (AccyPy 133, Micrometric) before and after crashing and milling the samples below 26 μm, respectively.

The results are the mean of three measurements. The experimental errors in the evaluations ρ_a, ρ_s and ρ_{as}, are ±0.03, ±0.01 and ±0.01 g cm^{-3} leading to mistakes of about 2% for total and open porosity and at about 1% for closed porosity, respectively. The experimental errors for LS and WA are ±0.5% and 1%, respectively.

The effect of composition and microstructure on the mechanical characteristics of the investigated new samples was studied using a combination of classical strength tests and micro-indentation tests.

The compressive strength (σ_c) was obtained by standard compression tests on cylindrical samples with a height to diameter ratio of two (h/D = 2). Three samples of each type were tested. The measurements were carried out using an electro-mechanical Instron 3300 (Instron, MA, USA).

Samples' hardness and Young's modulus of indentation were measured by depth-sensing micro-indentation (Depth-Sensing Vickers Microindenter, C.S.M. Instruments, Peseux, Switzerland). The continuous stiffness measurement continuously measured the stiffness and allowed the hardness and elastic modulus to be determined as continuous function of penetration depth. A maximum load of 10000 mN was set and it was reached applying a loading rate of 1500 mN min^{-1}, with 10 s holding time at the load necessary to reach the maximum displacement. Fifteen measurements were performed on different regions of three samples of each type and an average value was obtained. The hardness and the Young's modulus values for each sample were calculated according to the Oliver and Pharr methods, respectively (Oliver and Pharr, 1992).

Results and discussion

Sintering and phase formation

The densification behaviour of samples C and C–b (i.e. the variations of linear shrinkages versus temperature) is reported in Figure 2. Both dilatometric curves present a first linear shrinkage of about 0.5% at about 530 °C, which was related to the kaolinite deoxydrilation. After that, the sintering plot of the C–b sample presented a second linear shrinkage of about 3.5%, which started at ~850 °C and stopped at the beginning of the phase formation range (970 °C–980 °C). At the same time, this sintering step in C sample was related with a lower linear shrinkage of ~2.5%. Moreover, a third densification range, leading to shrinkage of 4.5% was observed in the range 1250 °C–1300 °C. Similar high temperature densification was, practically absents in C–b sample.

This difference in the sintering behaviour could be related to the presence of 4% residual organic phase in sample C. Most probably, during the heat-treatment, the burning of this residual organic phase leads to an increase of porosity and then a densification process happens with the formation of melt trapped inside the porosity.

The sintering process of C–b sample was studied also at 1100 °C, 1120 °C and 1130 °C for 1 h. The plots are shown in Figure 2(b) and highlight that no additional densification or significant expansion of the samples were carried out at these temperatures. These results clearly demonstrate that the heat-treatment for bricks sintering might be limited to the modest temperature of 1000 °C.

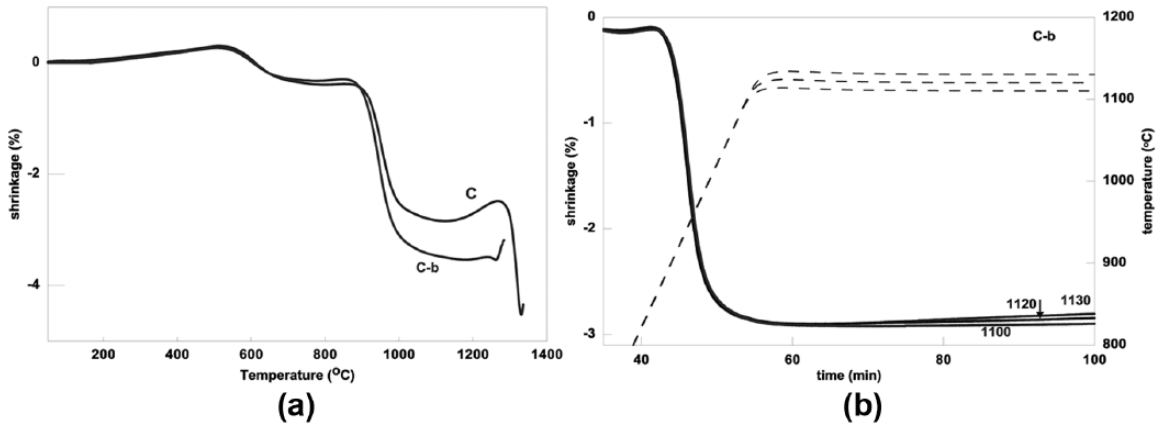

Figure 2. Dilatometer (DIL) curves of C and C–b compositions: (a) non-isothermal and (b) isothermal results at 1100 °C, 1120 °C and 1130 °C.

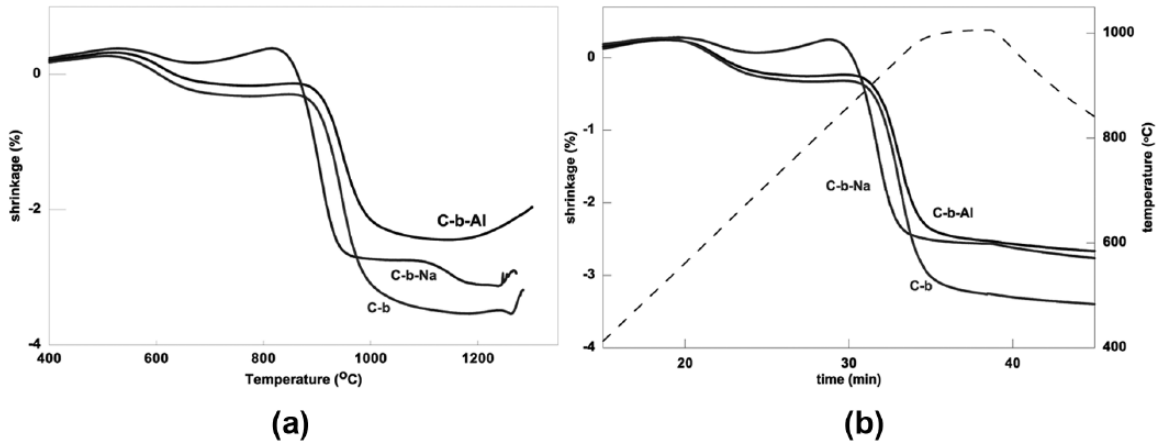

Figure 3. Dilatometer (DIL) curves of C–b, C–b–Al and C–b–Na compositions: (a) non-isothermal and (b) isothermal results after 5 min holding at 1000 °C.

The effects of the addition of Na_2CO_3 and Al_2O_3 (i.e. flux and inert reinforcement) in the C–b batch was also investigated by non-isothermal dilatometry and the sintering curves are reported in Figure 3(a). The decomposition of Na_2CO_3 at 700 °C–800 °C leads to some expansion but, after that, the formed Na_2O acts as a very intensive fluxing agent, decreasing the densification temperature with about 100 °C. At the same time, the addition of Al_2O_3 reduces the densification rate, which decreases the firing shrinkage by around 1%. The additional isothermal results (5 min at 1000 °C), which are presented in Figure 3(b), highlight that very short heat-treatment is needed to complete the densification process

The DTA plots of C–b, C–b–Al and C–b–Na are presented in Figure 4. The effects related to kaolinite deoxydrilation are identical for the all the compositions. The crystallisation exo-peaks, Tp, for samples C–b–Al and C–b were detected at 985 °C–980 °C, whereas the melting endo-effect occurred in the range of 1160 °C–1200 °C for both samples. The results demonstrated that the addition of an inert corundum fraction does not influence on the phase formation and melting processes. At the same time, the addition of 5 wt% of Na_2CO_3 leads to simultaneous decreasing of both crystallisation and melting temperatures with about 100 °C.

The comparison of non-isothermal DTA and dilatometry curves show that the low temperature partial densification is related to the neo-formation crystalline phase processes, while the secondary high temperature sintering and/or overfiring coincide with the melting of some neo-formed crystalline phases.

The DTA and dilatometry results also confirm that the low-cost heat-treatment schedule (5–10 min at 1000 °C) can be used for the samples densification.

Fired samples physico-mechanical properties

The physico-mechanical quality of fired briquette specimens was investigated to estimate the firing shrinkage, water absorption, weight loss on ignition of bricks, density and the load bearing capacity.

Water absorption (WA) gives information for open porosity. Low values imply good resistance to the natural environment and acceptable permeability of bricks. From the results in Table 5, it is clear the addition of Na_2CO_3 produces a decrease of brick WA. This can be explained by the difference in the open porosity of the mixtures. The WA for the C–b–Na sample is less with respect

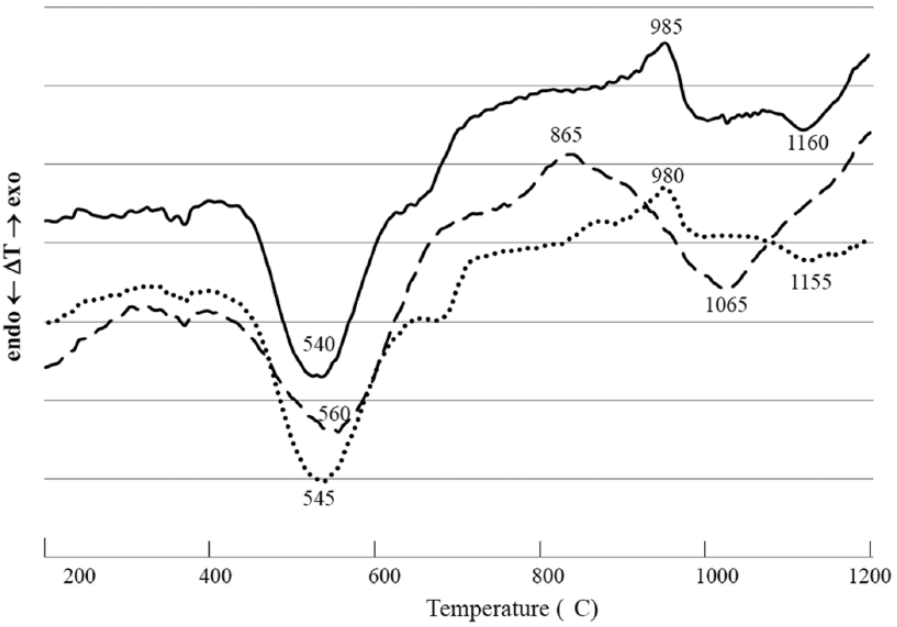

Figure 4. Non-isothermal DTA results of C–b (dot line), C–b–Al (solid line) and C–b–Na (dash line) ceramic batches.

Table 5. Technological properties: Compressive strength (σ_c), loss on ignition (WLOI%), linear shrinkage (LS%), water absorption (WA%), measured densities, hardness (H_{IT}) and indentation modulus (E_{IT}) for the fired samples.

Properties	C–b	C–b–Na	C–b–Al
σ_c (MPa)	55±6	33±1	59±6
WLOI (%)	7.3	10.6	6.9
LS (%)	4.0	3.5	3.5
WA (%)	14.5	11.5	13.0
ρ_a (g cm^{-3})	1.84	1.92	1.95
ρ_s (g cm^{-3})	2.67	2.62	2.77
ρ_{as} (g cm^{-3})	2.70	2.74	2.78
P_O (%)	31	26	30
P_C (%)	1.1	4.4	0.4
P_T (%)	32.0	30.0	30.0
H_{IT} (GPa)	0.80±0.35	1.41±0.50	1.75±0.24
E_{IT} (GPa)	16±3	22±5	19±2

to C–b and C–b–Al, because the formation of the Na_2O-enriched phase with low viscosity can reduce the open porosity, which corresponds to an increase of closed porosity.

Table 5 summarises the values of the weight of loss on ignition (WLOI) for the fired bricks. As reported by several works, the WLOI for a normal clay brick is 15% (Long Lin, 2006; Lissy and Sreeja, 2014). Based on Table 5, all the fired bricks have a lower WLOI. The C–b sample has low WLOI followed by C–b–Al with percentages of loss of 7.3% and 6.9%, respectively. The higher WLOI value, measured for the C–b–Na sample, was mainly owing to the contribution of Na_2CO_3 dissociation and gas evolution during the firing process in the temperature ranging from 700 °C to 800 °C.

The quality of brick could be further measured by examining the linear shrinkage (LS) of samples. Shrinkage in the ceramic process is a significant parameter, since structural change and solidification, implying densification, may create tensions and failures in fired bricks (Mekki et al., 2008). All the LS values obtained for the new fired bricks (Table 5) are lower than 4%. Furthermore, the progressive addition of Al_2O_3 and Na_2CO_3 produces a decrease of the sample's LS with respect to the C–b sample.

To investigate the load-bearing capacity of these new building materials, including the Al_2O_3 and Na_2CO_3 addition, a uniaxial-compressive loading test was carried out.

The results reported in Table 5 indicate that the incorporation of Na_2CO_3 and Al_2O_3 influence the strength of the bricks. Even if the C–b–Na sample has a higher density and lower open porosity, a decrease of the compressive strength was measured. The decreased compressive strength can arise, as reported in the next paragraph, from the new crystalline phases created, the albite phase to the detriment of anorthite. However, the compressive strength results range from 33 MPa in the C–b–Na sample, to 59 MPa in the C–b–Al sample. Depending on the countries, there are different standards specifying brick grades according to the compressive strength values. For instance, withdrawn European standards specify a minimum strength of 5 MPa for burnt clay bricks (BS 3921, 1985; TS 705, 1985).

All the samples of our study, made with BA–b, have compressive strengths comparable with the standard strength values. In fact, according to ASTM C-67 (1992), the minimum required compressive strength of a paving brick subjected to light traffic is 17.2–20.7 MPa (Loryuenyong et al., 2009).

From another point of view, ASTM C62 (2005), for building and facing bricks, respectively, correlate the compressive strength with the weathering resistance specifying a minimum value of 20.7 MPa, to not be susceptible to degradation. In these terms, all the samples in this study should be durable to severe weathering.

The mechanical behaviour is inherently linked to the microstructure and constituent properties at micro-scale. In order to quantify this link and correlate the effect of open and closed porosity on micromechanical properties, an indentation technique was used (Piatasik and Hasselman, 1964). This testing procedure, based on the traditional Vickers hardness measurement, is based on continuous monitoring of the load and displacement of the hard probe as it is driven and withdrawn from the material at discrete locations of a grid. The obtained load–displacement diagrams, not provided in the manuscript, allow the determination of the material hardness H_{IT} and indentation modulus E_{IT} (Krakowiak et al., 2011).

The values reported in Table 5 evidence an increase of indentation hardness (H_{IT}) and indentation Young modulus (E_{IT}) after the addition of Na_2CO_3 and Al_2O_3. At a sub-millimetre scale the fired bricks, obtained in this work, can be ascribed to form a porous composite material whose behaviour is driven by matrix and porosity. The increase of average micro-hardness and indentation Young modulus in the C–b–Na sample can be attributed to reduction of open porosity and increase of closed porosity. Moreover, the presence of a harder phase as Al_2O_3 enhances the hardness of the bricks matrix from 0.80 GPa to 1.75 GPa. Then, the average microhardness obtained for sintered C–b–Na and C–b–Al samples are more than a doubling of the microhardness compared with the C–b sample.

Phase assemblage and microstructure

The evolution of the phase composition during heating and then the characteristic feature of structural brick materials was studied by XRD analysis of the sample using a heating chamber. Figure 5 reports the spectra for C–b, C–b–Na and C–b–Al samples respectively, gathered during heating.

The spectra of initial ceramic batches correspond to the main crystalline phases of used raw materials (i.e. kaolinite, quartz, calcite and akermanite). The spectra of batches sintered at 900 °C, present alpha quartz [JCPDF file 01-082-0511] as the main crystalline phase and traces of ghelenite ($Ca_2Al(AlSi)O_7$) [JCPDF file 01-089-5917] deriving from the initial BA–b waste component. At 1000 °C, in agreement with the DTA results, which elucidated an intensive phase formation in the interval 900 °C–1000 °C, formation of anorthite ($CaAl_2Si_2O_8$) [JCPDF file 00-002-0523] was evidenced. In fact, in a heterogeneous system, such as the used BA (Lam et al., 2010), the alkaline oxides are the most reactive components, resulting in the formation of an intergranular thin liquid phase, involving mass transport phenomena giving rise to the formation of new phases, such as anorthite (Acchar et al., 2013).

The XRD results with the addition of Na_2CO_3 reflect some variations in the crystalline phases developed. As can be seen, the final stages of heating the formation of some albite ($NaAlSi_3O_8$) [JCPDF file 01-083-1610] is indicated. In fact, the addition of Na_2CO_3 leads to the formation of Na_2O (fluxing

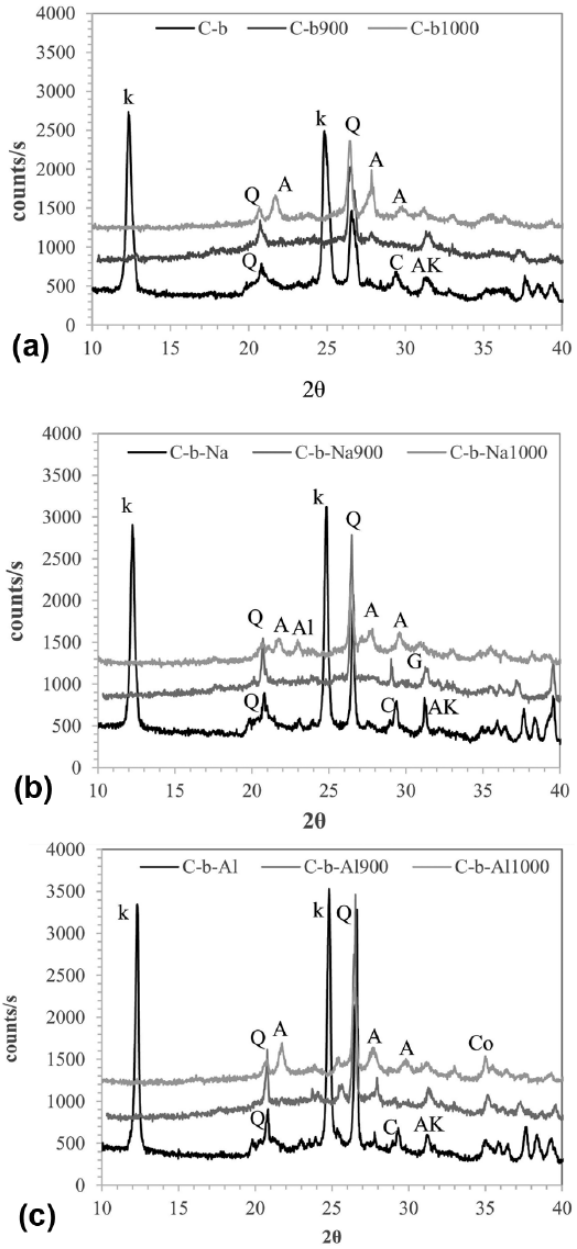

Figure 5. XRD spectra of (a) C–b, (b) C–b–Na and (c) C–b–Al ceramic batches at different temperatures.
Q: quartz; K: kaolinite; A: anorthite; G: ghelenite; C: calcite; AK: Akermanite, Al: Albite, Co: Corundum.

oxide) that accelerates the local melting and subsequent crystallisation. On the other hand, the presence of Al_2O_3 does not influence the formation of new crystalline phases and peaks of corundum with identical intensity are observed in all spectra. The increase, with the temperature, of the background signal can be attributed to the presence of an amorphous phase, for example aluminosilicate glasses.

The results of this qualitative analysis are supported by the SEM-EDS results. Figure 6 demonstrates typical images of the main crystal phases in the samples (together with the corresponding EDS spectra). Figure 6(a) and (b) show the main typical crystalline phases, anorthite and albite solid solution. Unreacted glass

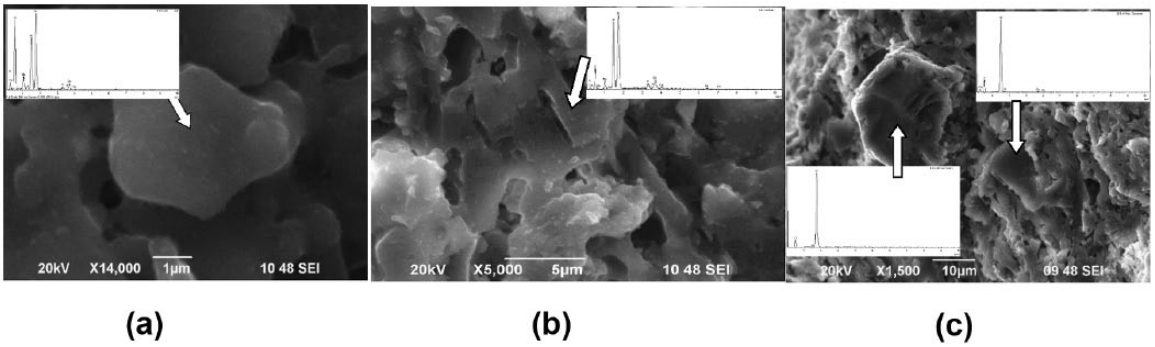

Figure 6. SEM images and EDS analysis of fractured surface of samples fired at 1000 °C: (a) C–b, (b) C–b–Na and (c) C–b–Al.

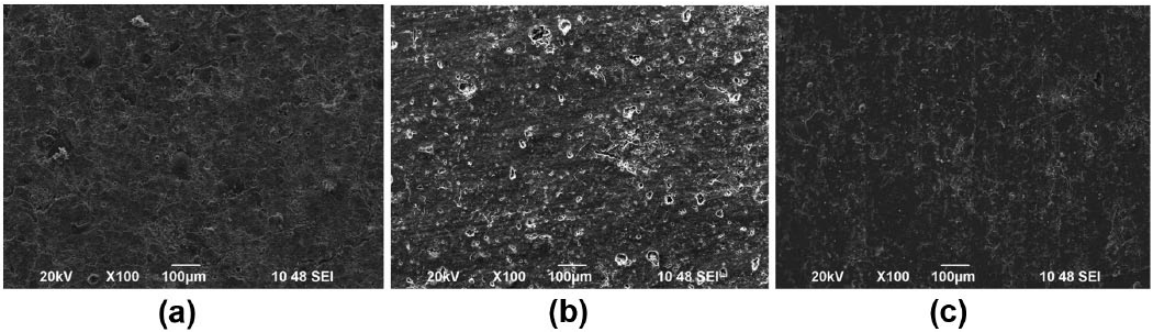

Figure 7. SEM images of samples surface fired at 1000 °C: (a) C–b, (b) C–b–Na and (c) C–b–Al.

particles, pyroxene, ghelenite and corundum particles, were also observed in C–b–Al sample (Figure 6(c)).

SEM images of the sample surfaces at low magnification, showing a ceramic body with a degree of sintering for brick production and typical open porosity (Karaman et al., 2001) are presented in Figure 7, respectively. Additionally, the SEM observations of the C–b sample fired at 1120 °C (not reported in the work) confirmed that no drastic structural charges were carried out when temperature is increased by 100 °C–120 °C.

Conclusion

The possibility to manufacture ceramic bricks by re-using of high amount of one inert material, generated from MSWIs, is demonstrated.

It is shown that, during a low-cost treatment (5–10 min at about 1000 °C), some densification and intensive re-crystallisation reactions between the meta-kaolinite and the phases from BA were carried out. It is also demonstrated that the addition of Na_2CO_3 results in the decrease of sintering and re-crystallisation temperatures, resulting in a reduction of open porosity as well as to some variations in the crystalline phases developed. At the same time, no effect in the phase formation was observed with Al_2O_3 addition.

The low firing shrinkage coupled with low WLOI and the improved mechanical properties (all of obtained samples have sufficient compressive strength over 20 MPa) demonstrated the high potential of pre-treated MSW BA to be used as a clay substitute to produce good face solid bricks.

Declaration of conflicting interests

The authors declared no potential conflicts of interest with respect to the research, authorship, and/or publication of this article.

Funding

The authors received no financial support for the research, authorship, and/or publication of this article.

ORCID iD

R Taurino https://orcid.org/0000-0001-7834-9948

References

Acchar W, Dultra EJV and Segadães AM (2013) Untreated coffee husk ashes used as flux in ceramic tiles. *Applied Clay Science* 75–76: 141–147.

Aineto M, Acosta A and Iglesias I (2006) The role of a coal gasification fly ash as clay additive in building ceramic. *Journal of the European Ceramic Society* 26: 3783–3787.

Aloisi M, Karamanov A, Taglieri G, et al. (2006) Sintered glass ceramic composites from vitrified municipal solid waste bottom ashes. *Journal of Hazardous Material* B137: 138–143.

Asenov St, Lakov L and Toncheva Kr (2013) Promising ceramic materials for ballistic protection. *Journal of Hazardous Material* 48: 190–195.

ASTM C-67 (1992) Standard Test Method of Sampling and Testing Brick and Structural Clay Tile.

ASTM C62 (2005) Standard Specification for Building Brick (Solid Masonary Units from Clay of Shale).

Barbieri L, Andreola F, Lancellotti I, et al. (2013) Management of agricultural biomass wastes: Preliminary study on characterization and valorisation in clay matrix bricks. *Waste Management* 33: 2307–2315.

BS 3921 (1985) Specification for Clay Bricks, British Standard.

Cultrone G, Sebastian E, Cazalla O, et al. (1998) Physical, mineralogical and textural features of ceramic clays from Granada Province (Spain).

In: Gomes CSF (Ed.) Proceedings of the second Mediterranean clay meeting, Aveiro, Portugal, 16–19 September, pp.298–303.

Cultrone G, Sebastian E and de la Torre MJ (2005) Mineralogical and physical behaviour of solid bricks with additives. *Construction and Building Materials* 19: 39–48.

Demir I (2006) An investigation on the production of construction brick with processed waste tea. *Building and Environment* 38: 1451–1455.

Dermates D and Meng X (2003) Utilization of fly ash for stabilization/solidification of heavy metal contaminated soils. *Engineering Geology* 70: 377–394.

EN 12457-2 (2002) Characterization of Waste. Leaching Compliance Test for Leaching of Granular Waste Materials and Sludge.

He H, Yue Q, Qi Y, et al. (2012) The effect of incorporation of red mud on the properties of clay ceramic bodies. *Applied Clay Science* 70: 67–73.

He P, Zhang H, Zhang CG, et al. (2004) Characteristics of air pollution control residues of MSW incineration plant in Shanghai. *Journal of Hazardous Material* 116: 229–237.

Huang WJ and Chu SC (2003) A study on the cementlike properties of municipal waste inceneration ashes. *Cement Concrete Resource* 33: 1795–1799.

ISO 10545-3 (1995) Determination of Water Absorption, Apparent Porosity, Apparent Relative Density and Bulk Density.

ISPRA-Istituto Superiore per la Protezione e la Ricerca Ambientale (2008) Waste Report. Available at: http://www.apat.gov.it/site/it-T/APAT/Pubblicazioni/RapportoRifiuti (accessed 10 December 2008).

Karaman S, Ersahin S and Gunal H (2001) Firing temperature and firing time influence on mechanical and physical properties of clay bricks. *Journal of the European Ceramic Society* 21: 1073–1080.

Krakowiak KJ, Lourenço PB and Ulm FJ (2011) Multitechnique investigation of extruded clay brick microstrucyure. *Journal of the American Ceramic Society* 94: 3012–3022.

Lam CHK, Ip AWM, Barford JP, et al. (2010) Use of incineration MSW ash: A review. *Sustainability* 2: 1943–1968.

Lingling X, Wei G, Tao W, et al. (2005) Study on fired bricks with replacing clay by fly ash in high volume ratio. *Construction Building Materials* 19: 243–247.

Lissy MPN and Sreeja MS (2014) Utilization of sludge in manufacturing energy efficient bricks. *IOSR Journal of Mechanical and Civil Engineering* 11: 70–73.

Little MR, Adell V, Boccaccini AR, et al. (2008) Production of novel ceramic materials from coal fly ash and metal finishing wastes. *Resources, Conservation and Recycling* 52: 1329–1335.

Long Lin K (2006) Feasibility study of using brick made from municipal solid waste incinerator fly ash slag. *Journal of Hazardous Materials* B137: 1810–1816.

Loryuenyong V, Panyachai T, Kaewsimork K, et al. (2009) Effects of recycled glass substitution on the physical and mechanical properties of clay bricks. *Waste Management* 29: 2717–2721.

Mandal AK and Sinha OP (2017a) Effect of bottom ash fineness on properties of red mud geopolymer. *Journal of Waste Technology and Management* 43: 26–35.

Mandal AK and Sinha OP (2017b) Preparation and characterization of fired bricks made from bottom ash and iron slime. *Journal of Materials in Civil Engineering* 29. Epub ahead of print 4 April 2017. DOI: http://dx.doi.org/101061/(ASCE)MT.1943–5533.0001767.

Martínez-García C, Eliche-Quesada D, Pérez-Villarejo L, et al. (2012) Sludge valorization from wastewater treatment plant to its application on the ceramic industry. *Journal of Environmental Management* 95: 343–348.

Mekki H, Anderson M, Benzina M, et al. (2008) Valorization of olive mill wastewater by its incorporation in building bricks. Journal of Hazardous Materials 158: 308–315.

Menezes RR, Ferreira HS and Neves GA (2005) Use of granite sawing wastes in the production of ceramic bricks and tiles. *Journal of the European Ceramic Society* 25: 1149–1158.

Monteiro SN (2005) Effect of oily waste addition to clay ceramic. *Ceramics International* 31: 353–358.

Mular AL, Halbe DN and Barratt DJ (2002) Mineral Processing Plant Design, Control and Practice Proceedings, Vol.1, Vancouver, British Columbia: SME.

Muñoz PV, Morales MPO, Letelier VG, et al. (2016) Fired clay bricks made by adding wastes: Assessment of the impact on physical, mechanical and thermal properties. *Construction and Building Materials* 125: 241–252.

Naganathan S, Razak HA and Nadzrian AH (2011) Effect of kaolin addition on the performance of controlled low-strength material using industrial waste incineration bottom ash. *Waste Management & Research* 28: 848–860.

Oliver WC and Pharr GM (1992) An improved technique for determining hardness and elastic modulus using load and displacement sensing indentation experiments. *Journal of Materials Research* 7: 1564–1583.

Paganelli M (1997) Understanding the behaviour of glazes: New test possibilities using the automatic hot stage microscope "Misura". *Industrial Ceramics* 17: 69–73.

Pan JR, Huang C, Kuo JJ, et al. (2008) Recycling MSW bottom ash and fly ash as raw materials for Portland cement. *Waste Management* 28: 1113–1118.

Pérez-Villarejo L, Eliche-Quesada D, Iglesias-Godino Fco J, et al. (2012) Recycling of ash from biomass incinerator in clay matrix to produce ceramic bricks. *Journal of Environmental Management* 95: 349–354.

Peters T and Iberg R (1978) Mineral changes during firing of calcium-rich brick clays. *American Ceramic Society Bulletin* 57: 503–509.

Piatasik RS and Hasselman DPH (1964) Effect of open and closed pores on Young's modulus of polycrystalline ceramics. *Journal of the American Ceramic Society* 47: 50–52.

Raut SP, Sedmake R, Dhunde S, et al. (2012) Reuse of recycle paper mill waste in energy absorbing light weight bricks. *Construction of Building Materials* 27: 247–251.

Sena da Fonseca B, Galhano C and Seixas D (2015) Technical feasibility of reusing coal combustion by-products from a thermoelectric power plant in the manufacture of fired clay bricks. *Applied Clay Science* 104: 189–195.

Sena da Fonseca B, Vilão A, Galhano C, et al. (2011) Reusing coffee waste in manufacture of ceramics for construction. *Advances in Applied Ceramics* 110: 225–232.

Schabback LM, Andreola F, Barbieri L, et al. (2012) Post treated incinerator bottom ash as alternative raw materials for ceramic manufacturing. *Journal of the European Cearmic Society* 32: 2843–2852.

Sokolar R and Vodova L (2011) The effect of fluidized fly ash on the properties of dry pressed ceramic tiles based on fly ash–clay body. *Ceramics International* 37: 2879–2885.

TS 705 (1985) Solid brick and vertically perforated bricks. Turkish Standard.